ELECTRON BEAM DYNAMICS IN THE LONG-PULSE, HIGH-CURRENT DARHT-II LINEAR INDUCTION ACCELERATOR

Carl Ekdahl, E. O. Abeyta, P. Aragon, R. Archuleta, G. Cook, D. Dalmas, K. Esquibel, R. Gallegos, R. Garnett, J. Harrison, J. Johnson, E. Jacquez, B. Trent McCuistian, N. Montoya, S. Nath, K.Nielsen, D. Oro, L. Rowton, M. Sanchez, R. Scarpetti, M. Schauer, G. Seitz, V. Smith, and R. Temple, Los Alamos National Laboratory, Los Alamos, NM 87545, USA

R. Anaya, G. Caporaso, F. Chambers, Y.J. Chen, S. Falabella, G. Guethlein, B. Raymond, R. Richardson, J. Watson, and J. Weir, Lawrence Livermore National Laboratory, Livermore, CA 94550, USA

H. Bender, W. Broste, C. Carlson, D. Frayer, D. Johnson, C. Y. Tom, C. Trainham, and J. Williams, NSTec, Los Alamos, NM 87544, USA

B. Prichard and M. Schulze, SAIC, San Diego, CA 92121, USA

T. Genoni, T. Hughes, and C. Thoma, Voss Scientific, Albuquerque, NM 87108, USA

Abstract

The DARHT-II linear induction accelerator (LIA) now accelerates 2-kA electron beams to more than 17 MeV. This LIA is unique in that the accelerated current pulse width is greater than 2 microseconds. This pulse has a flat-top region where the final electron kinetic energy varies by less than 1% for more than 1.5 microseconds. The long risetime of the 6-cell injector current pulse is 0.5 µs, which can be scraped off in a beam-head cleanup zone before entering the 68-cell main accelerator. We discuss our experience with tuning this novel accelerator; and present data for the resulting beam transport and dynamics. We also present beam stability data, and relate these to previous stability experiments at lower current and energy.

INTRODUCTION

The Dual-Axis Radiography for Hydrodynamic Testing (DARHT) facility has two linear induction accelerators (LIAs) for flash radiography to provide orthogonal views of explosive hydrodynamic experiments. The 2-kA, 20-MeV Axis-I LIA has been producing radiographs with a single 60-ns pulse since the year 2000. We have now operated the 74-cell Axis-II LIA at 2 kA and 17 MeV. The Axis-II LIA is unique in that its beam pulse has a long, 1.6-µs flattop during which the kinetic energy varies by less than ±1%. A kicker cleaves up to four short pulses out of this long pulse, and these are converted to bremsstrahlung radiation for multi-pulse radiography.

The long-pulse 2-kA beam was produced in a 2.5-MV diode powered by a Marx generator. A diverter switch (crowbar) is incorporated at the Marx output to shorten the >2-µs pulse to have a flat-top between 0.200-µs and 2.0-µs. After leaving the diode, the beam is accelerated by six induction cells to ~3.5 MeV. Each cell has a focusing

solenoid for beam transport, as well as dipoles for beam steering. Apertures downstream of the injector cells can be used to scrape off the long off-energy beam head by changing the magnetic field of the preceding two or three solenoids. For most of the experiments described here this beam-head clean-up zone (BCUZ) was configured to pass almost the entire beam head, just as in earlier tests [1,2,3]. The main LIA has 68 induction cells that have been upgraded to provide enough potential to accelerate the beam to more than 17 MeV. Each of these main accelerator cells also has a focusing a solenoid and steering dipoles. The solenoids through the main accelerator were tuned to transport a matched beam through a field increasing to more than 1 kG on axis to suppress the beam breakup (BBU) instability. After exiting the accelerator, the kicker slices the beam into short pulses, and the downstream transport system (DST) focuses these pulselets onto the bremsstrahlung radiation converter to produce up to four radiography source spots [4]. The DST includes solenoid and quadrupole focusing elements, as well as steering dipoles.

The tunes for the DARHT-II magnetic transport were designed with two envelope codes, XTR [5] and LAMDA [6]. These solve the same beam-envelope differential equations, keeping terms that are neglected in the usual paraxial approximation [7]. The difference between the two codes is mostly that LAMDA has the capability for time varying envelope simulations. LAMDA also has the capability to handle elliptical beams, and was used extensively to design tunes for the downstream transport [4]. Using these codes, a magnetic field tune was designed with a strong enough magnetic field to suppress beam breakup (BBU). The tune and resulting envelope are shown in Figure 1.

Solution of the second-order differential envelope equations requires initial conditions for the beam radius

and convergence. Because of the difficulty of access to the diode for direct measurements of initial conditions, we have relied on simulations of the space-charge limited diode using the TRAK gun-design code [8] and the LSP particle-in-cell code [9]. Figure 2 shows a TRAK simulation for the full 2.5-MV diode voltage. The initial conditions for the envelope codes are determined from TRAK and LSP at ~80 cm downstream from the cathode surface.
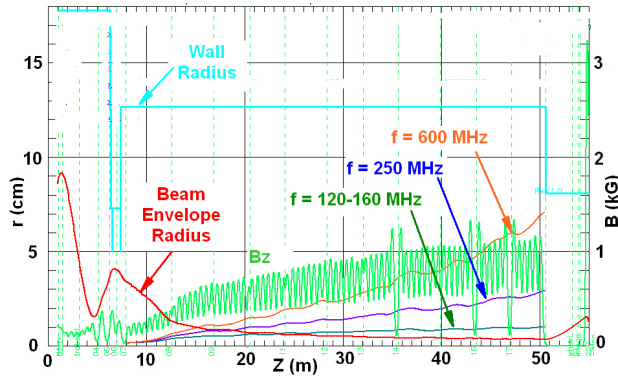

Figure 1: Beam envelope as calculated by XTR for our tune. Also shown is the saturated growth of the three principal modes of BBU for a 50-micron initial perturbation. The locations of BPMs are shown as vertical green dotted lines.
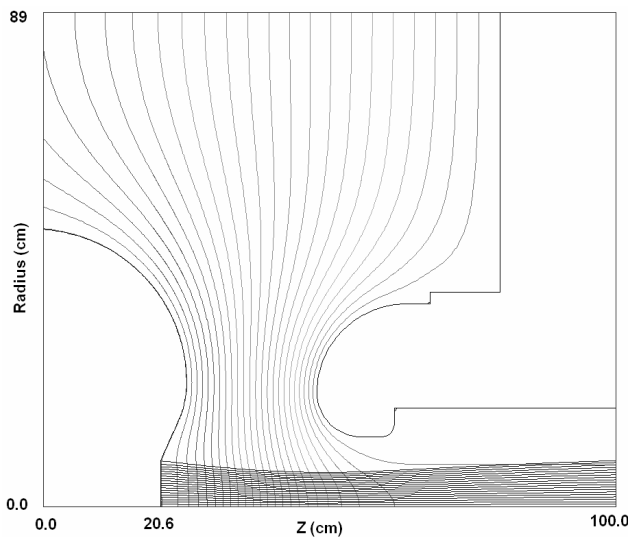

Figure 2: TRAK simulation of space-charge limited current emitted by the hot dispenser cathode in the Axis-II diode. The initial conditions for the envelope codes are obtained at the right hand edge of this plot.

The initial conditions, the space-charge limited current, and the normalized emittance were obtained from the simulations for impressed diode AK voltages in 100 kV steps from 100 kV through 2.8 MV so that the envelope codes could be used to predict beam behavior during the long, ~500–ns risetime. This was necessary to design the

tune through the injector cells so that none of the off-energy electrons in the beam head were lost, even in the absence of accelerating fields.

EXPERIMENTAL RESULTS

Non-invasive DARHT-II beam diagnostics, such as beam position monitors (BPMs), were used on every shot [2,3]. In addition to beam position, the BPMs provide beam current and ellipticity data. Eighteen BPMs were located throughout the accelerator as shown in Fig. 1 to provide current and position data. Only the BPMs at the accelerator exit had the eight detectors required to provide unequivocal ellipticity measurements [2,10]. Most of the 12 BPMs in the downstream transport had eight detectors for ellipticity measurements because of the quadrupoles located there. Invasive diagnostics were only occasionally used. These included a magnetic spectrometer to measure beam-electron kinetic energy, and time-resolved imaging of the beam current profile using Cerenkov emitters [1,2,4,11].

We could not directly validate the diode simulations with experimental data because of the difficulty of access to the diode exit for measuring beam size. So we indirectly confirmed the TRAK/LSP predictions of radius and convergence during the beam risetime by adjusting the last of the injector solenoids to scrape off most of the off-energy beam head with the BCUZ apertures. Measurements of beam current after the BCUZ were in close agreement with the LAMDA time dependent envelope simulation (Fig. 3). For this injector tune, the predicted beam loss in the BCUZ is exceptionally sensitive to initial conditions used by the envelope codes, so these data are convincing evidence for the validity of the PIC and ray-trace simulations of the diode.
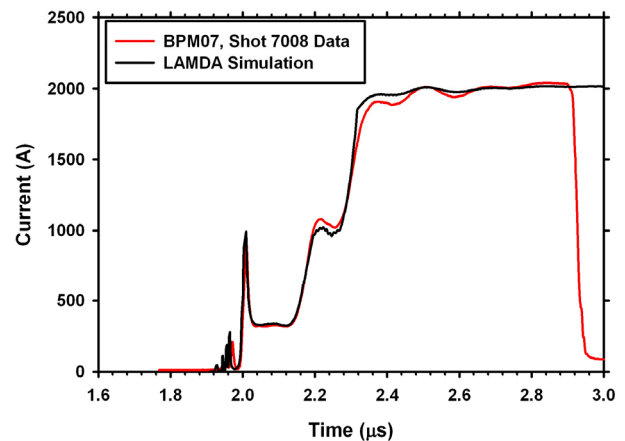

Figure. 3: Beam current transported through the BCUZ. Red curve: Experimental data from BPM measurement. Black curve: Lamda simulation using TRAK/LSP initial conditions that vary with diode voltage, and the measured diode voltage waveform.

There was no measurable loss of flattop beam current through the LIA. Figure 4 is an overlay of BPM

measurements throughout the injector and accelerator for a single shot. The < 1.5% scatter in average flattop current is consistent with experimental uncertainty, and uncorrelated with beam loss. The nominal injector tune for these experiments causes only slight beam loss in the BCUZ during the risetime, unlike the tune used to validate the diode simulations (Fig. 3) which deliberately scraped off most of the beam head. The ~7-MHz oscillation on the beam head was the result of large capacitances and inductances on the diode structure [1]. The current was terminated by the closing of the crowbar switch, which was timed to coincide with the end of the accelerating cell pulse. The red cursors in Fig. 4 delineate the 1.6-μs flattop used for the four radiography pulses. Figure 5 shows the electron kinetic energy measured with our magnetic spectrometer. The kinetic energy of the accelerated beam exceeds 17.0 MeV for more than 1.6 μs. For this measurement, five of the LIA cells were turned off, which reduced the energy by ~1.3 MeV from that expected with all 74 cells.
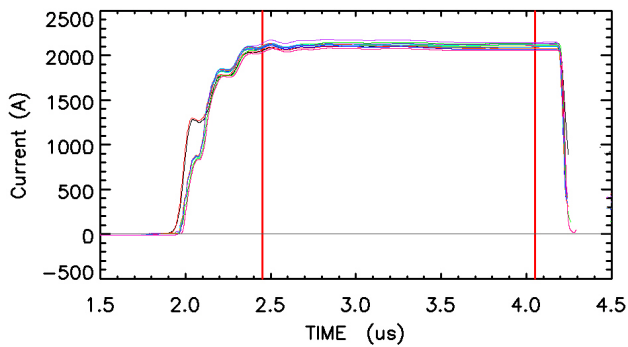

Figure 4: Overlay of beam current measurements in injector and accelerator. Red cursors indicate the 1.6-μs flattop region used for the four radiography pulses.
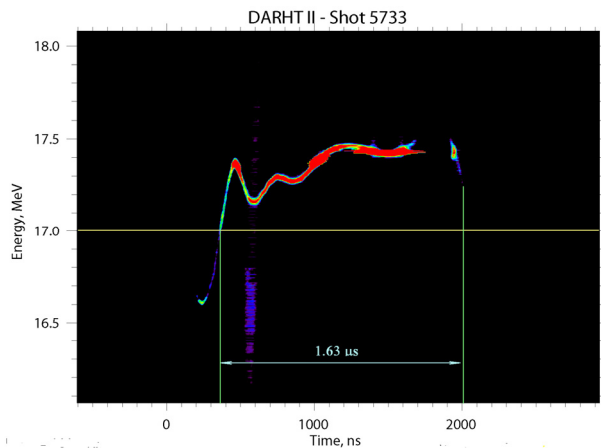

Figure 5: Magnetic spectrometer measurement of electron kinetic energy.

Beam motion at the exit of the accelerator was dominated by an energy dependent sweep, with ~5.7-mm amplitude over the 1.6-μs flattop. Beam sweep is undesirable because it effects the locations of the four

radiography pulses, so we must understand it, and reduce its amplitude. While head-to-tail sweep is a characteristic of the resistive wall instability, we believe it unlikely that this instability is responsible for the sweep observed at the exit of Axis-II. In a uniform strong solenoidal focusing field, the distance for an initial perturbation to exponentiate is approximately $L = 3.1Ba^3/I_b/(\tau\rho)^{1/2}$, where a is the pipe radius in cm, B is the field in kG, I_b is the beam current in kA, τ is the pulse-length in μs, and ρ is the pipe resistivity in μΩ-cm [12]. The growth is independent of energy, in contradiction to our sweep data, which show a strong correlation with the beam energy variation illustrated in Fig. 5. Moreover, we estimate that the growth of an initial perturbation in DARHT-II is less than 60% over the length of the LIA. Therefore, it is unlikely that the sweep is caused by resistive wall instability.

Another cause of sweep is corkscrew, or the interaction of the energy-varying beam with a few accidental dipoles from cell misalignment. Indeed, the observed sweep amplitude can be fit to a model of dipole deflection resulting from the observed energy variation (Fig. 5). Suppression of corkscrew by using steering dipoles has been demonstrated on other LIAs [13]. In an initial attempt to reduce our sweep amplitude, we used only a few of the available steering dipoles. We were able to reduce the sweep amplitude acceptable for commissioning the multi-pulse radiography target, and for our first radiographs of an upcoming hydrodynamic test. This initial attempt reduced the sweep amplitude by ~40% to ~3.3-mm amplitude over the 1.6-μs flat top [14]. We anticipate further improvements in the future by using more of our dipoles.
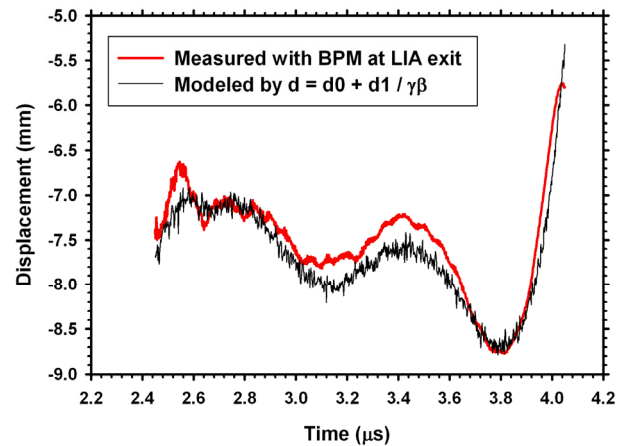

Figure 6: Comparison of measurements with a model of sweep caused by energy variation interacting with a single accidental dipole. Red curve: displacement measured with BPM at exit. Black curve: displacement calculated from energy variation (Fig. 5) and dipole model.

For the DARHT-II LIA the BBU amplitude saturates at $\xi(z)=(\gamma_0/\gamma)^{1/2}\xi_0\exp(\Gamma_m)$, where subscript zero denotes

initial conditions, and γ is the usual relativistic mass factor [3]. The maximum growth exponent is $\Gamma_m = I_b N_g Z_\perp <1/B> / 3 \times 10^4$ [15]. Here I_b is the beam current in kA, N_g is the number of gaps, the transverse impedance $Z_\perp$ is in Ω/m, and the average focusing force $<1/B>$ is in kG^{-1}. This theoretical prediction was confirmed in earlier experiments with legacy cells [3], and those results were used to design a tune with magnetic field strong enough to suppress the BBU to an amplitude < 10% of beam radius (Fig. 1). We recorded the beam position data at the accelerator exit (BPM20) at 5 Gs/s to have enough bandwidth to resolve even the highest frequency BBU mode. Figure 7 shows the beam position at the accelerator exit during a 200-ns window near the end of the beam pulse. High frequency BBU is clearly present, but the amplitude is less than 60 microns, which is <10% of the predicted beam radius (> 3 mm) at that location.
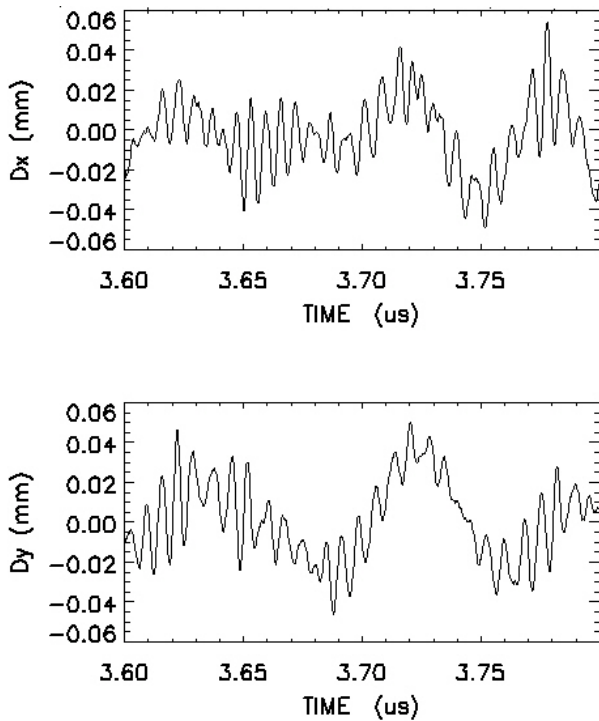

Figure 7: Beam position at accelerator exit. These data have the sweep filtered out to emphasize the BBU and the lower frequency oscillation thought to result from the ion hose instability. The predicted beam radius at this position is > 3 mm.

Figure 8 shows a spectral analysis of the beam motion at the accelerator exit. In addition to the activity at the lower BBU frequencies, BBU activity at the highest frequency mode (~600 MHz) can be clearly seen, now that we have high enough bandwidth recording. The BBU signal at 600 MHz does not appear to be as strong as might be expected from the transverse impedance measurements due to the bandwidth limitations of our BPMs and their long signal cables. The observed BBU

with this tune agrees with the earlier measurements and with the theory as shown in Fig. 9.

We also observed beam motion in the 10-20 MHz range characteristic of ion hose [3], which is likely the result of gas generated in the BCUZ by the slight scraping of the beam head (Fig. 4).
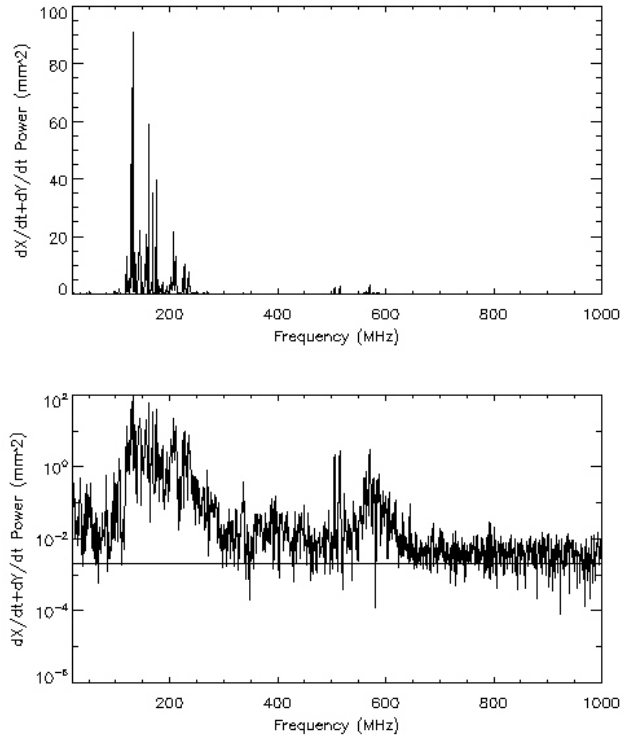

Figure 8: BBU frequency analysis of beam transverse motion at the accelerator exit shows BBU activity in the 600-MHz band, as well as in the previously observed lower frequency bands [3].
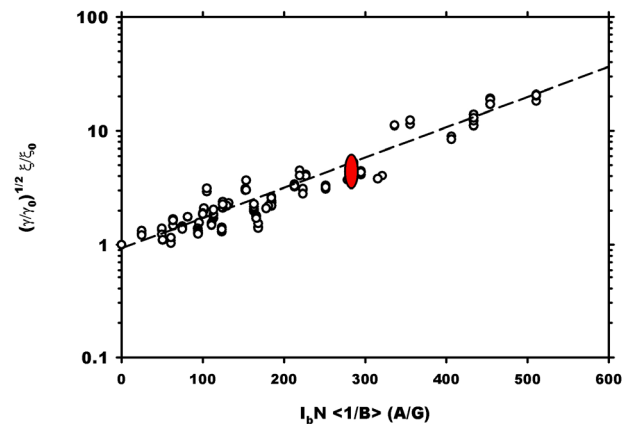

Figure 9: BBU growth. Open circles: data obtained in low-current, low-energy experiments[3]. Filled oval: range of data obtained during these experiments with the 2-kA, 17-MeV accelerator.

After exiting the accelerator, the kicker sliced four short pulses out of the long accelerator pulse. These were

transported to the bremsstrahlung converter with little loss as shown in Fig. 10. The resulting radiographic spots were imaged using the same pinhole based, time resolved spot size diagnostic used to measure the Axis-I spot [17].
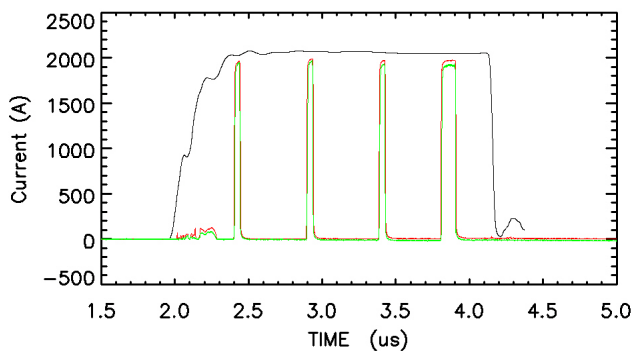

Figure 10: Overlay of data from BPMs throughout the accelerator and downstream transport showing the accelerator-current pulse and the kicked-current pulses.

The four radiography source spots produced by Axis-II were comparable to the Axis-I spot. Los Alamos characterizes radiography source spots by comparing the modulation transfer function (MTF) of the source spot with the MTF of a uniformly illuminated disk. The spot size is defined as the diameter of the disk that has the same MTF half width as the source spot. Sizes of the four Axis-II spots averaged 1.7±0.2 mm [4], which compare favorably with the 1.8±0.1-mm Axis-I spot [17] used for radiography since year 2000.

In conclusion, we operated the DARHT-II accelerator at its fully rated current, energy, and pulse width. Even at the full 2-kA current, the solenoidal magnetic field of the tune was strong enough to suppress the BBU to acceptable amplitude. Low amplitude ion hose motion was also observed. The beam motion at the exit was dominated by beam sweep. After some additional steering to reduce the sweep, the beam was stable enough for us to commission the multi-pulse kicker, downstream transport and radiography target.

REFERENCES

[1] Carl Ekdahl, et al., "First beam at DARHT-II," in Proc. 2003 Part. Accel. Conf., (2003), pp. 558-562.

[2] Carl Ekdahl, et al., "Initial electron-beam results from the DARHT-II linear induction accelerator," IEEE Trans. Plasma Sci. 33, (2005), pp. 892-900.

[3] Carl Ekdahl, et al., "Long-pulse beam stability experiments on the DARHT-II linear induction accelerator," IEEE Trans. Plasma Sci. 34, (2006), pp.460-466.

[4] Martin Schulze, et al., "Commissioning the DARHT-II Accelerator Downstream Transport and Target," in Proc. 2008 Linear Accel. Conf., (2008) , p. 427-429.

[5] Thomas P. Hughes, David C. Moir and Paul W. Allison, "Beam injector and transport calculations for ITS," in Proc. 1995 Part. Accel. Conf., (1995), pp. 1207-1209.

[6] Thomas .P. Hughes, et al., "LAMDA User's Manual and Reference", Voss Scientific technical report VSL-0707, April 2007.

[7] E. P. Lee and R. K. Cooper, "General envelope equation for cylindrically symmetric charged-particle beams," Part. Acc. 7, (1976), pp. 83-95.

[8] Stanley Humphries Jr., "TRAK – Charged particle tracking in electric and magnetic fields," in Computational Accelerator Physics, R. Ryne Ed., New York: American Institute of Physics, (1994), pp. 597-601.

[9] T. P. Hughes, R. E. Clark, and S. S. Yu, "Three-dimensional calculations for a 4 kA, 3.5 MV, 2 microsecond injector with asymmetric power feed," Phys. Rev. ST Accel. Beams 2, (1999), pp. 110401-1 – 110401-6.

[10] Carl Ekdahl, "Aliasing errors in measurements of beam position and ellipticity," Rev. Sci. Instrum. 76, (2005), pp.095108-1 – 095108-9.

[11] H. Bender, et al., "Quasi-anamorphic optical imaging system with tomographic reconstruction for electron beam imaging," Rev. Sci. Instrum. 78, (2007), pp. 013301.

[12] G. J. Caporaso, W. A. Barletta, and V. K. Neil, "Transverse resistive wall instability of a relativistic electron beam," Particle Accelerators, vol. 11, (1980), pp. 71-79.

[13] J. T. Weir, J. K. Boyd, Y.-J. Chen, J. C. Clark, D. L. Lager, and A. C. Paul, "Improved ETA-II accelerator performance," in Proc. 1999 Particle Accelerator Conf., (1999), pp. 3513-3515.

[14] Carl Ekdahl, et al., "Electron beam dynamics in the long-pulse, high-current DARHT-II linear induction accelerator," in Proc. 2008 European Part. Accel Conf., (2008) pp. 968-970.

[15] V. K. Neil, L. S. Hall, and R. K. Cooper, "Further theoretical studies of the beam breakup instability," Particle Accelerators, vol. 9, (1979), pp. 213-222.

[16] R. Briggs and W. Waldron, "Transverse impedance measurements of the modified DARHT-2 accelerator cell design," LBNL Report #59199, November, 2005.

[17] B. T. McCuistian, et al., "Temporal spot evolution of the DARHT first axis radiographic spot," in Proc. 2008 European Part. Accel Conf., (2008) pp. 1206-1208.